Pergamon

0956-7151(94)E0052-I

Acta metall. mater. Vol. 42, No. 7, pp. 2219–2231, 1994

0956-7151/94 $7.00 + 0.00

MICROBUCKLE PROPAGATION IN CARBON FIBRE-EPOXY COMPOSITES

M. P. F. SUTCLIFFE and N. A. FLECK

Engineering Department, Cambridge University, Trumpington Street, Cambridge CB2 1PZ, England

(Received 19 January 1994)

Abstract—Observations of microbuckle propagation in uni-directional carbon fibre-epoxy material are described. The fibres buckle either in the plane of the specimen or out-of-plane, depending on the constraints on the free surface. Large scale bridging models of in-plane and out-of-plane microbuckles are reported. The in-plane and out-of-plane microbuckles are modelled as mode II and mode I cracks, respectively. Sliding behind the microbuckle tip is resisted by a constant shear stress of 90 MPa for the in-plane microbuckle, and by a constant normal stress of 220 MPa for the out-of-plane microbuckle. For both the in-plane and out-of-plane microbuckles a microbuckle tip toughness in the range 10–17 kJ/m^2 is inferred from the experiments. The observed relative displacements across an out-of-plane microbuckle agree with theoretical values using the mode I bridging model. Micrographs of the propagating microbuckle tip show that the details of the failure mechanism are similar for both in-plane and out-of-plane microbuckling. Both develop kink bands with a width of between 25 and 70 μm and with a propagation angle β of between 25° and 30°. A process zone extends about 250 μm ahead of the kink band tip, wherein the fibres buckle and break. Fibres in this region become almost straight again on unloading. When the deduced large scale bridging model of microbuckling failure for unidirectional material is applied to failure at a sharpened slit in multi-directional laminates, reasonable agreement is found between the theoretical and the observed compressive fracture toughnesses.

1. INTRODUCTION

Carbon fibre reinforced plastics are increasingly being used in primary load-bearing structures where they are subjected to both tensile and compressive loading. The need to design with small safety factors while at the same time ensuring reliability requires a sound understanding of failure mechanisms. This paper is concerned with the compressive failure of these materials.

The observed failure mechanisms in compression depend upon both the specimen geometry and the lay-up of the composite. Damage development can be divided into two stages, an initiation stage and a propagation stage. Initiation depends on the details of the specimen geometry at the fibre scale. For example, initiation for specimens with a slit† depends on the root radius. In notched specimens containing a hole or slit, both initiation and subsequent stable damage growth are observed [1, 2]. For unnotched specimens with either uni- or multi-directional lay-ups a stable initial stage is not observed. This is because damage growth is unstable (under both fixed remote load and fixed remote displacements) and subsequent failure obliterates any initial damage.

†Relatively blunt slits sharpened at the end with a razor blade are used for compression testing to prevent closure of the slit faces while still generating a large stress concentration factor at the slit tip.

1.1. Microbuckling in uni-directional laminates

Notched uni-directional specimens loaded along the fibre direction normally fail by splitting along the fibre direction at the ends of the notches. Unnotched uni-directional specimens fail by plastic microbuckling [1]. Budiansky and Fleck [3] propose an infinite band model for microbuckling. Figure 1 illustrates the geometry of the kink band. Loading is in the fibre direction. The transverse direction may be either the through-thickness direction of the panel, in which case Fig. 1 represents an "out-of-plane" microbuckle, or it may lie in the plane of the panel; Fig. 1 then represents an "in-plane" microbuckle. In carbon fibre epoxy composites the kink band is defined by a line of fibre breaks at each boundary of the band, forming a band with a width w of between 10 and 15 fibre diameters. Fibres within the infinite band are given an initial imperfection in the form of an initial fibre rotation $\bar{\phi}$. Budiansky and Fleck calculate the collapse response of this kink band, and give the variation of remote applied stress σ_r with additional fibre rotation ϕ, neglecting any effects of fibre bending. Fleck *et al.* [4] refine this model by introducing fibre bending. The infinite band models are clearly applicable when a coherent region of initial waviness spans a large proportion of the specimen. However Hahn and Williams [5] suggest, based on observations of partially formed microbuckles, that microbuckles in unnotched specimens in fact form by propagation of a kink band from an initial defect or

from the free edge. Similar partially formed kink bands in a carbon-carbon composite are described by Adler and Evans [6]. It is not clear how to apply an infinite band model either to initiation at a small defect or to the propagation process. In particular the induced waviness associated with strain gradients ahead of a propagating microbuckle may overshadow the effects of initial fibre waviness. Fleck and Budiansky [7] assumed that a microbuckle propagates like a dislocation. The Burgers vector of the dislocation is the shear displacement across the boundaries of the microbuckle as a result of fibre rotation within the microbuckle band. There are at least two competing mechanisms by which a microbuckle may propagate: (i) as a dislocation, and (ii) as a crack. The focus of the current paper is to present experimental support for the notion that a microbuckle in a carbon fibre reinforced epoxy laminate propagates in a similar manner to that of a crack.

1.2. Microbuckling in multi-directional laminates

Multi-directional laminates containing a mixture of ply orientations are used in practical applications to give adequate strength and stiffness in more than one direction. These laminates exhibit a number of failure mechanisms in compression for both the notched and unnotched geometry. These include splitting along the fibre directions, delamination between plies, matrix plasticity in the off-axis plies and microbuckling of the main load bearing axial plies which are aligned with the loading direction [1, 2, 8].

Soutis *et al.* [9] find that the strain-to-failure of unnotched multi-directional laminates is close to that of uni-directional specimens. Noting that, for uni-directional material, microbuckling is the only failure mechanism, they infer that microbuckling is the dominant failure mechanism in multi-directional laminates. Chang and Lessard [10] model laminate failure using a layered finite element damage model. While considering different damage mechanisms in the laminate, they do not model the details of the microbuckle. Soutis *et al.* [9] predict the strength of specimens with a central hole by measuring a laminate compressive fracture toughness using a slit geometry and applying a large scale bridging analysis. The microbuckle is modelled by assuming that there is no stress intensity factor at the tip of the microbuckle and that the stresses across the propagating microbuckle obey a simple linear softening relationship between the stress behind the microbuckle and the displacements across it. The success of this model can be explained by the similarity in failure modes between the slit and hole geometries. However, the model relies on experimental data for the laminate toughness. Ideally this laminate toughness would itself be predicted from uni-directional data or directly from the properties of the fibres and matrix.

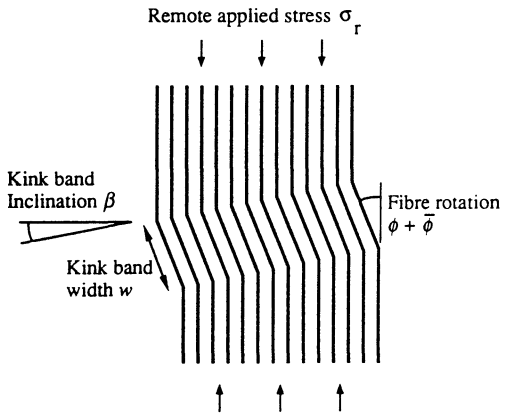

Fig. 1. Infinite band model of microbuckling.

1.3. Scope of the paper

In the foregoing introduction a variety of cases have been described—notched and unnotched specimens made from uni- and multi-directional lay-ups; in most cases, the dominant failure mechanism is microbuckle propagation. The outline of the paper is as follows. Large scale bridging models are used to described both in-plane and out-of plane microbuckle propagation in uni-directional materials. A small process zone at the tip of the microbuckle is modelled by a tip toughness. Behind the microbuckle tip it is assumed that the microbuckle faces can transmit a constant shear stress for in-plane microbuckling, and a constant normal stress for out-of-plane microbuckling. Experimental observations and measurements are described which support this model. The crack bridging model is then applied, in a crude way, to model the failure of multi-directional specimens. The tip toughness and bridging traction measurements described in the paper supply experimental data for future theoretical models and also supply the required information for direct use of a large scale bridging model for notched laminates. Although damage initiation is particularly important in unnotched specimens, that topic is beyond the scope of the paper.

2. MICROBUCKLE PROPAGATION IN UNI-DIRECTIONAL MATERIAL: A CRACK BRIDGING MODEL

In this section we describe a large scale crack bridging model for in-plane and out-of-plane microbuckle propagation; in the following Section 3 experimental measurements are summarised which support the applicability of the crack bridging model.

2.1. Crack bridging model for in-plane microbuckling

Consider first the in-plane microbuckle. Figure 2(a) shows a schematic view of the bridging model. Fibres rotate within the microbuckle band until the fibres "pile-up" against each other: volume conservation ensures that the normal displacement across the microbuckle vanishes [3]. The microbuckle zone is treated as a sliding crack, such that the flanks of the

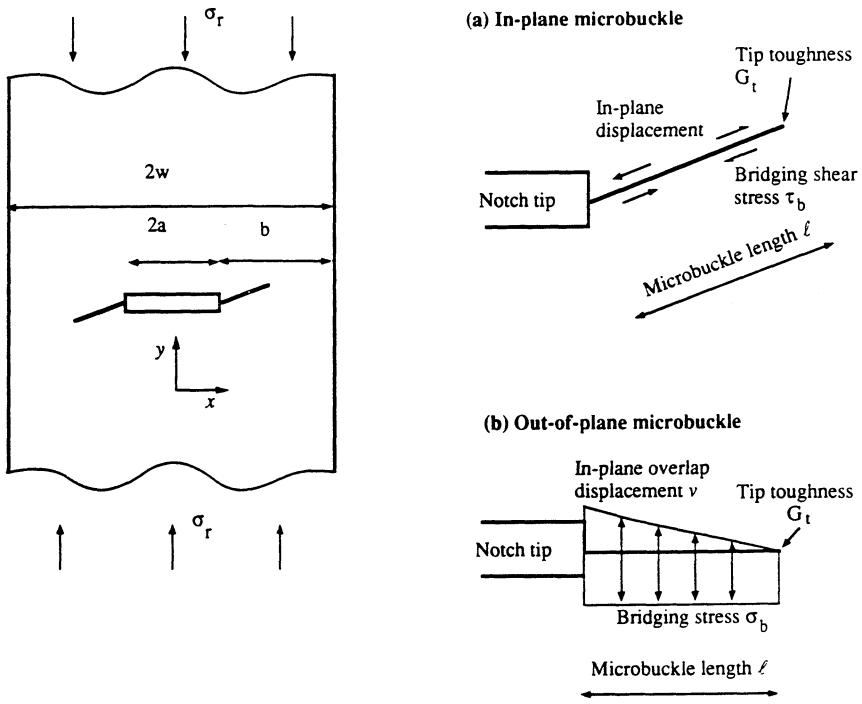

Fig. 2. The large scale bridging model: (a) for an in-plane microbuckle: (b) for an out-of-plane microbuckle.

microbuckle transmit a constant bridging shear stress τ_b, and the tip of the microbuckle has a tip toughness G_t. The model is implemented using the finite element method. Further details are given in Section 3.4, and details of the finite element scheme are given in Appendix A.

2.2. Crack bridging model for out-of-plane microbuckling

The out-of-plane microbuckle shown in Fig. 2(b) is modelled as a compressive mode I crack, with a compressive tip toughness G_t and a constant compressive bridging traction σ_b in a direction normal to the faces of the crack. Figure 2(b) shows a schematic view of the bridging model. The in-plane displacement component v shown in Fig. 2(b) appears as an apparent overlap of the crack. It is assumed that, although there are out-of-plane displacements which allow this apparent overlap of material, these can neglected in this analysis. The normal bridging traction σ_b on the crack faces is associated with the resistance to sliding of the microbuckle faces and is taken to be constant. Implementation of this crack bridging model is described in Section 3.5; full details of the model are given in Appendix B.

3. CALIBRATION OF THE CRACK BRIDGING MODEL FROM COMPRESSION EXPERIMENTS

Notched, uni-directional specimens of carbon fibre epoxy composite were loaded in compression in order to elucidate the details of microbuckle propagation. The tests also served to estimate the microbuckle tip toughness for both in-plane and out-of-plane microbuckling. The magnitude of the bridging stresses across the microbuckle was estimated in independent experiments reported in Section 4.

3.1. Experimental method

To investigate microbuckle propagation in unidirectional material, the specimen geometry in Fig. 3 was used. Loading was along the fibre direction. The composite was made of 24 plies of T800/924C carbon fibre-epoxy giving a thickness of 3 mm. Elastic constants for the material are given in Table 1. The specimen was loaded through aluminium end tabs glued onto the front and back faces of the specimen. Further details of the loading arrangement are given in [1]. A notch perpendicular to the fibre and loading direction was cut in the specimen using either a saw blade, or by spark erosion, giving a slit about 0.5 mm thick. This was sharpened at the tip using a razor blade.

Uni-directional specimens generally fail by splitting at the tips of the transverse notch. However one specimen split from the middle of the main notch and then microbuckled at the notch tip. To encourage this behaviour, subsequent specimens had an additional notch cut in them along the fibre direction as shown in Fig. 3.

Euler buckling of the specimen was prevented by an anti-buckling guide. This guide lightly clamped a 7 mm wide strip adjacent to each edge of the specimen, as shown in Fig. 3, to limit out-of-plane deformation and so avoid macro-buckling. However, small

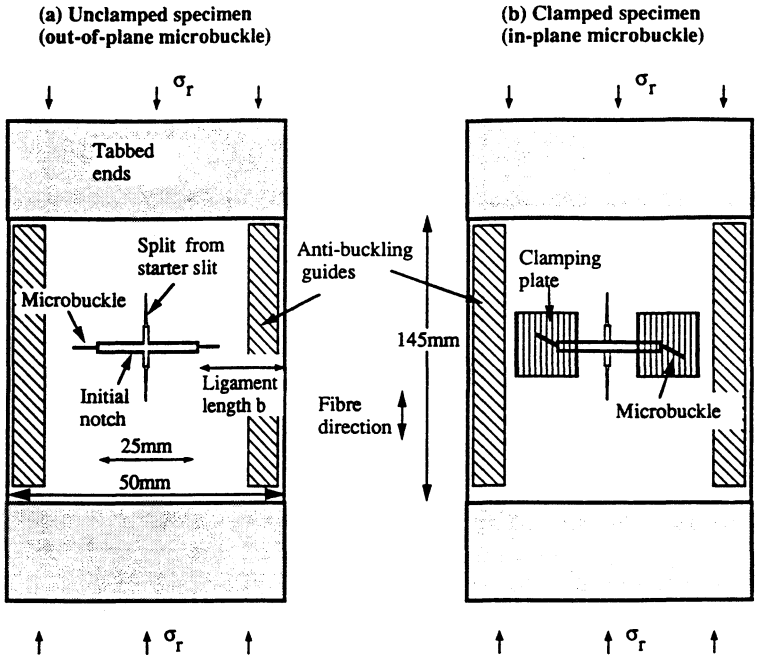

Fig. 3. The specimen geometry used to propagate microbuckles in uni-directional material: (a) unclamped specimen (out-of-plane microbuckle); (b) clamped specimen (in-plane microbuckle).

out-of-plane displacements at the notch tip were not prevented. In some tests, small square plates were used to clamp the free surfaces at the notch tip, as illustrated in Fig. 3(b), and thus prevent out-of-plane movement. The average clamping pressure was about 50 MPa. These specimens shall be referred to as "clamped specimens".

The specimen was loaded under displacement control using a cross-head speed of 3×10^{-3} mm s^{-1}. Peridically loading was interrupted to measure the length of the microbuckles at each end of the notch. Values quoted are an average of these two lengths. Although the difference in lengths was significant (in the extreme one microbuckle was twice the length of the other), the high repeatability of the results in terms of applied stress versus average microbuckle length indicates that this is not a cause of significant error.

3.2. *Observed microbuckle geometries*

Microbuckles grew from the tips of the notches of both the clamped and unclamped specimens. These microbuckles propagated across the specimen in a stable way under displacement loading.

Optical and scanning electron microscopy was used to observe the mechanism of microbuckle propagation across the ligament of the specimens.

Figure 4(a) gives a schematic view of the propagating microbuckle geometry for the clamped specimen.

Table 1. Elastic constants for the uni-directional T800/924C material

E_{xx}(GPa)	E_{yy}(GPa)	G_{xy}(GPa)	ν_{xy}	E'(GPa)
9.25	161	6	0.0195	54.8

Relative displacements across the microbuckle are in the plane of the specimen—this is an in-plane microbuckle. The microbuckle propagates at a β angle of about 25° to the transverse direction. The propagation front is parallel to the through-thickness direction.

Figure 4(b) shows a schematic view of the microbuckle geometry for the unclamped specimen. There is relative sliding on the faces of the microbuckle leading to out-of-plane displacements—this is an out-of-plane microbuckle. Displacements across the microbuckle can be resolved into a component w normal to the plane of the specimen and a component v in the plane of the specimen and parallel to the loading (and fibre) direction. The microbuckle propagates in the transverse direction but is inclined at a β angle of approximately 30° to the through-thickness direction.

In both types of microbuckle there is continued relative sliding across the microbuckle behind the microbuckle tip. More detailed observations of the tip region of propagating in-plane and out-of-plane microbuckles are given in Section 4.

3.3. *Observed variation of microbuckle length with load*

The variation of microbuckle length l with remote applied stress σ_r is given in Fig. 5 for a clamped specimen containing an in-plane microbuckle and for two unclamped specimens. The microbuckle length is normalised by the original unnotched ligament length b, which is 12.5 mm. The clamped specimen carries a significantly higher load than the unclamped specimens, both at the initiation of damage and as the

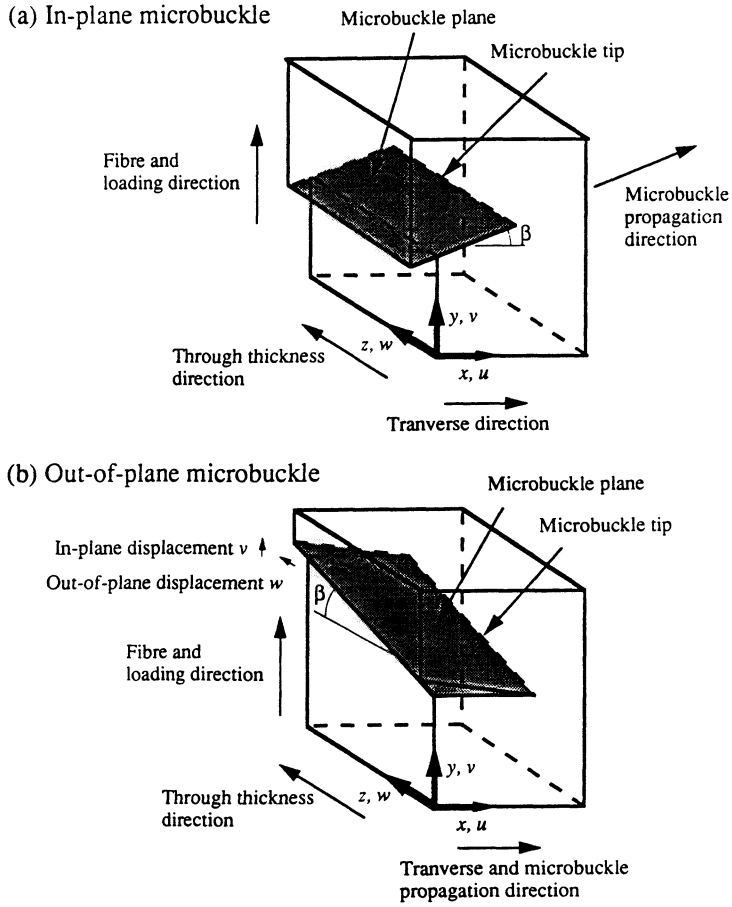

Fig. 4. Schematic of the propagating microbuckle geometry; (a) for an in-plane microbuckle; (b) for an out-of-plane microbuckle.

microbuckle propagates across the specimen. Out-of-plane microbuckle growth remains stable as the microbuckle traverses the ligament of the unclamped specimen, but results for l/b greater than 0.8 have been omitted due to the extra lateral support provided by the anti-buckling guide beyond this point.

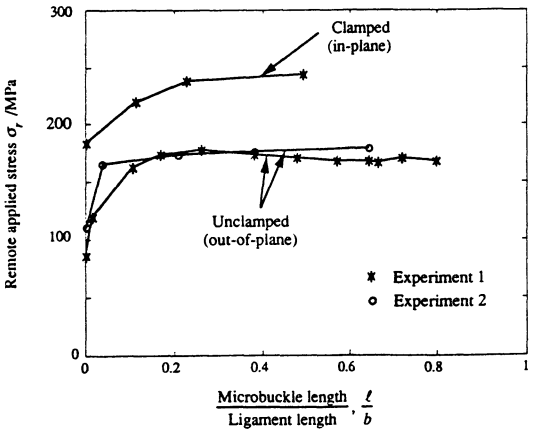

Fig. 5. The variation of applied load with microbuckle length for clamped and unclamped specimens (the ligament length b is 12.5 mm).

3.4. *Inferred tip toughness for an in-plane microbuckle*

For a given specimen geometry, microbuckle length l, remote applied stress σ_r and bridging stress τ_b, the inferred tip toughness of the microbuckle can be found from an elastic calculation. This calculation is done using the finite element method, implemented using ABAQUS [11]. Details of the calculations are given in Appendix A.

The observed response of microbuckle length l vs remote applied stress σ_r is used to give a series of estimates for the microbuckle tip toughness. After initiation we expect the tip toughness to be a constant. Figure 6 shows the inferred tip toughness as a function of microbuckle length assuming (i) $\tau_b = 0$ MPa, and (ii) $\tau_b = 90$ MPa. The notch is 0.5 mm wide, so that we can expect the notch to have some effect for microbuckles of length less than about 1.5 mm ($l/b = 0.12$). The difference between curves for $\tau_b = 0$ MPa and $\tau_b = 90$ MPa shows that bridging stress shields the microbuckle tip considerably. Using the "best estimate" of shear stress τ_b from Section 4.2. of 90 MPa we find that the estimated tip toughness rises from a value of 10 kJ/m^2 for $l/b = 0.12$ to a value of 17 kJ/m^2 for $l/b = 0.5$. The effect of assuming other values for τ_b can be calculated by using the

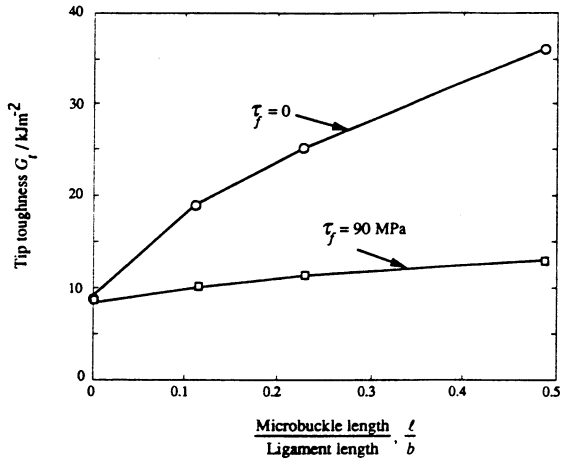

Fig. 6. The experimentally deduced toughness at the tip of an in-plane microbuckle.

approximation that the increase in inferred G_t from the curve for $\tau_b = 0$ scales as the square of the bridging stress τ_b. (Appendix A gives further details.)

It is useful to assess the effect of various modelling assumptions on the estimated tip toughness. As well as uncertainty about the value of friction stress, which may lie between 50 and 130 MPa, we should also consider the effect of the frictional forces imposed by the side clamping plates. Assume that the clamping plates, loading over an area 7.5 mm above and below the microbuckle, have a friction coefficient on the composite surface of 0.15. The normal clamping stress of 50 MPa then corresponds to an increase in frictional stress τ_b of about 20 MPa acting on the 3 mm thick faces of the microbuckle and a corresponding reduction in the estimate of the tip toughness.

3.5. Inferred tip toughness for an out-of-plane microbuckle

In similar manner to that described for the in-plane microbuckle, we infer a series of estimates of G_t as the microbuckle grows, from the observed response of microbuckle length l vs remote applied stress σ_r. We expect G_t to be a material property independent of microbuckle length, after an initiation phase. At any measured microbuckle length l, the toughness G_t is inferred from the measured load assuming a constant value for the crack bridging traction σ_b. Independent measurements of σ_b are reported in Section 4.2, and we find that $\sigma_b = 220$ MPa.

Figure 7 shows the inferred values for G_t as a function of microbuckle length l, deduced from the measured remote load and by assuming a constant bridging traction of $\sigma_b = 220$ MPa. The tip toughness is found to be roughly constant at about 11 kJ/m^2. This is close to the values found for the in-plane microbuckle of between 10 and 17 kJ/m^2. The bridging stress makes a significant difference to the estimated tip toughness, as can be seen from the inferred tip toughness assuming $\sigma_b = 0$. The effect of errors in estimating the bridging stress can be estimated by using the fact that G_t scales in an approximately quadratic fashion with the assumed bridging stress σ_b (Appendix B gives further details).

3.6. Comparison of theoretical out-of-plane microbuckle displacements with measured values

To confirm the accuracy of the mode I large scale bridging model for out-of-plane microbuckling, measurements of displacements across the microbuckle were compared with theoretical values calculated using the measured remote load and the assumed crack bridging stress of $\sigma_b = 220$ MPa. Two critical tests were performed as follows.

In the first test, measurements were taken of the closing displacements at one of the notch tips in an unclamped specimen. The specimen geometry has already been given in Fig. 2. Displacements were measured in the loading direction using a travelling microscope. (Associated out-of-plane displacements were not measured.) The notch tip closing displacement was measured for the loaded specimen and values were recorded as a function of increasing microbuckle length, as shown in Fig. 8. Theoretical values of the microbuckle displacement corresponding to a tip toughness of $G_t = 11$ kJ/m^2 and a crack bridging stress $\sigma_b = 220$ MPa were calculated using the large scale bridging mode. The predictions are included in Fig. 8 and show excellent agreement between calculated and measured values of notch closing displacement. With increasing microbuckle length, there is continued relative movement behind the microbuckle tip with no region of "sticking". This supports the theoretical treatment of the microbuckle as a crack, rather than as a dislocation.

In the second test two lines were scribed on the surface of the specimen using a precision diamond tipped tool. The lines were 1.5 mm above and below the line of the notch, running parallel to the notch direction. The microbuckle grew away from the notch

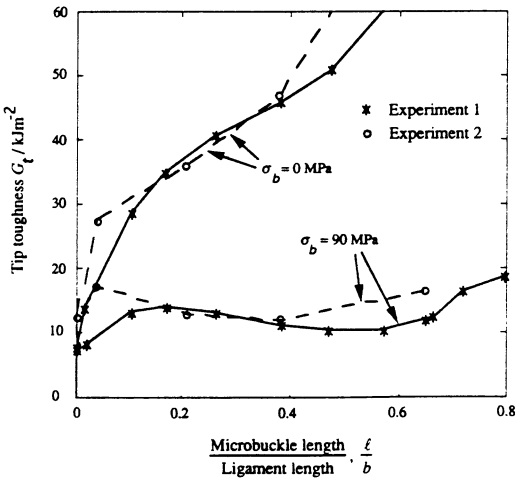

Fig. 7. The experimentally deduced toughness at the tip of an out-of-plane microbuckle.

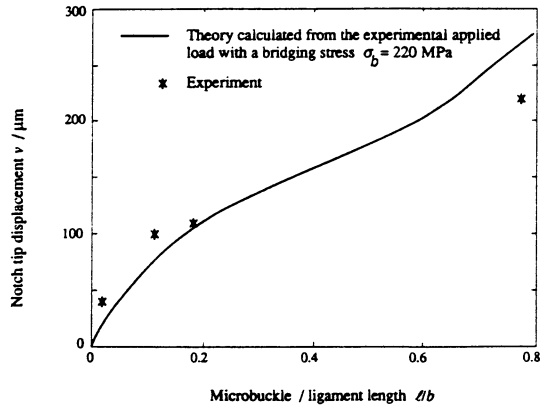

Fig. 8. Comparison of the theoretical and experimental values of the closing displacement v at the notch tip for an out-of-plane microbuckle.

between the lines spaced 1.5 mm above and below the notch. The relative displacement of these lines then gives a good estimate of the relative in-plane displacement across the microbuckle. Theoretical estimates of the closing displacement along the microbuckle (using the out-of-plane large scale bridging model with $G_t = 11$ kJ/m^2 and $\sigma_b = 220$ MPa) are compared with measurements in Fig. 9, for the case where the microbuckle has grown 0.44 of the way across the ligament ($l/b = 0.44$). The good agreement between the measured and calculated relative displacements along the microbuckle shown in Fig. 9 confirms the accuracy of the mode I model.

In Fig. 9 the closing displacement is taken as the relative displacement of the grid lines 1.5 mm on either side of the microbuckle. In the wake of the growing microbuckle the elastic displacements between the two scribed lines is of the order of 6 μm, which is much less than the magnitude of the closing displacements between the two scribed lines.

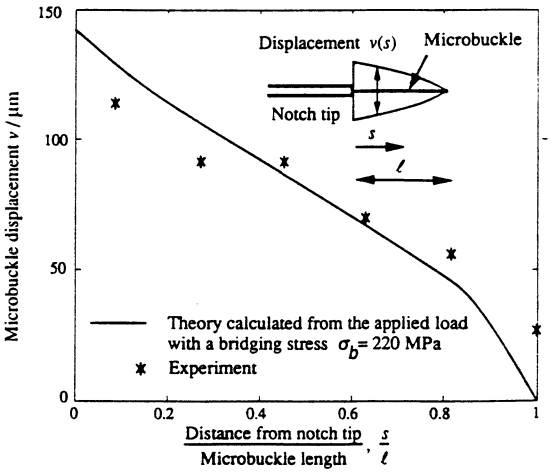

Fig. 9. Comparison of the theoretical and experimental values of the microbuckle closing displacement v for an out-of-plane microbuckle with $l/b = 0.44$ ($l = 5.5$ mm, $b = 12.5$ mm, $\sigma_r = 157$ MPa).

4. DETAILED SUPPORT FOR THE MICROBUCKLE BRIDGING MODEL

We have described in Section 2 a large scale bridging model of microbuckle propagation which assumes a tip process zone with a corresponding tip toughness, and a region behind the tip with a constant bridging stress and continuous sliding. In order to be able to separate the toughening process into a tip toughness and a bridging zone, we should show that there is a process zone at the tip of the microbuckle which is short compared to the propagating microbuckle length. Section 4.1 describes observations of the propagation tip and the region behind the tip which confirm these assumptions. Section 4.2 describes experiments to measure the bridging stress assumed in the large scale bridging analysis.

4.1. In situ observations of microbuckle propagation

Observations of the damage mechanisms were made by sectioning unloaded specimens, and by directly viewing the surface of loaded specimens either in a scanning electron microscope (SEM) or by using a travelling microscope. To produce specimens which could be loaded in the SEM, small sections of material which included the tip of a microbuckle were carefully cut from a specimen of the type shown in Fig. 2.

4.1.1. An in-plane microbuckle tip. Figure 10(a) shows a micrograph of the tip of an unloaded in-plane microbuckle. The split at the microbuckle tip is a result of unloading. Note that there are three or four broken fibres ahead of the kink band. This specimen was then re-loaded *in situ* in the SEM. Figure 10(b) shows a micrograph of the loaded microbuckle tip. Loading is in the fibre direction and the microbuckle is propagating from left to right. Scales are given on the micrographs. Although damage grew initially by propagation of a split from the microbuckle tip, further loading propagated the pre-existing microbuckle in-plane. The presence of the pre-existing microbuckle evidently generated stresses at the microbuckle tip conducive to this in-plane microbuckling. The kink band was between 25 and 35 μm in width and the microbuckle propagated at an inclination $\beta \approx 25°$ to the transverse direction. Figure 10(b) shows a region 100 μm ahead of the first broken fibre where the fibres are considerably bent but unbroken. There are occasional matrix cracks or voids between some of the bent fibres seen in Fig. 10(b). These cracks allow dilation associated with fibre rotation. Extensive crack growth was observed in the kink band after fibre fracture as the broken fibres underwent considerable further rotation. The "lock-up" condition observed in Fig. 10(a), where the fibres in the broken kink band have rotated by twice the angle of the kink band propagation angle β, corresponds to the rotation at which the dilation in the matrix returns to zero.

Fig. 10. The tip of an in-plane microbuckle. Loading and fibres run in the verical direction. (a) Unloaded: a split (A) runs from the tip of the microbuckle; (b) under load: the microbuckle is propagating from left to right.

Further fibre rotation is prevented by the limited compressibility of the matrix and fibre.

Figure 10(a), showing the unloaded tip, suggests that the distance behind the microbuckle tip from first fibre fracture to lock-up is of the order of a few kink band widths. The material on either side of the microbuckle behind the microbuckle tip slid on one of the fracture planes after the broken fibres had locked up. During unloading, the fibres ahead of the kink band and fibres in the kink band suffer small elastic rotations.

Generation of an in-plane microbuckle proved difficult to repeat; the preferred mode of failure is out-of-plane and the development of an in-plane microbuckle appears to be sensitive to the initiation conditions. However optical microscope observations of another clamped specimen showed a similar in-plane microbuckle on one face of the material. This test confirmed the details observed in the SEM. The zone containing fibres bent by more than about 1° extended between 200 and 400 μm ahead of the region where fibres were first broken. Any smaller fibre rotations further ahead of the microbuckle tip were obscured by the random waviness in the fibres.

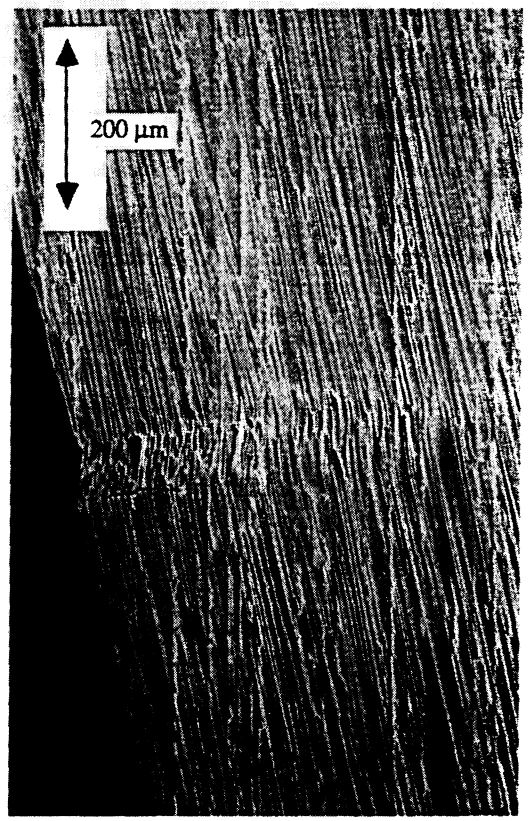

Fig. 11. An out-of-plane microbuckle under load. Loading and fibres run in the vertical direction. The microbuckle is propagating from left to right. The specimen is viewed from an angle of about 50° to the normal from the surface, so that distances in the propagation direction are fore-shortened by a factor of about 0.6.

4.1.2. An out-of-plane microbuckle tip. Figure 11 shows a scanning electron micrograph of an out-of-plane microbuckle. The specimen is viewed at an angle to the surface so that out-of-plane movement can be seen. The orientation of the specimen is such as to fore-shorten the lengths in the propagation direction (left to right in the micrograph) by a factor of 0.6. Lengths in the fibre direction are undistorted. The specimen is loaded *in situ* and the tip has just started to propagate. The out-of-plane movement at the edge of the specimen is clearly visible, as is a short kink band region about 70 μm in width. The surface of the specimen had been polished when unloaded, so that the region where fibres were bent out-of-plane ahead of the fibre fracture zone in the unloaded condition is delineated by the series of fibre ends seen in Fig. 11. The picture is similar to that for the in-plane test, with bent fibres extending a distance of about 250 μm ahead of the kink band.

On unloading the unbroken fibres straightened considerably, but still showed some residual waviness. This is in contrast to the in-plane microbuckle, where splitting mode I cracks between fibres seem to have enabled complete straightening of unbroken fibres [Fig. 10(a)]. The corresponding split for the out-of-plane microbuckle geometry would be a mode II shear crack. The absence of this crack is probably due to the greater toughness of mode II cracks as compared with mode I cracks. The difference in unloading mechanisms suggests that we should expect different fatigue behaviour for the two types of microbuckling.

4.2. Estimates of the microbuckle bridging stresses

We have seen that, behind the microbuckle tip, the assumption that the microbuckle flanks carry a constant stress gives good agreement with measurements of load and displacements. For the in-plane microbuckle we have taken a shear stress of 90 MPa; for the out-of-plane microbuckle we have assumed that the microbuckle carries a normal stress of 220 MPa, corresponding to a shear stress of 90 MPa on the flanks. In this section we describe supporting evidence for these assumptions.

4.2.1. Direct measurement of the normal traction in the wake of a growing microbuckle. To investigate the stresses carried across the microbuckle, strain gauges were placed on an unclamped specimen near the tip of the notch, as shown in Fig. 12. The specimen geometry has been given already in Fig. 2, and the strain gauge locations are shown in Fig. 12. Material under the strain gauges loaded elastically, so that the stresses at these locations could be inferred from the elastic modulus of the material.

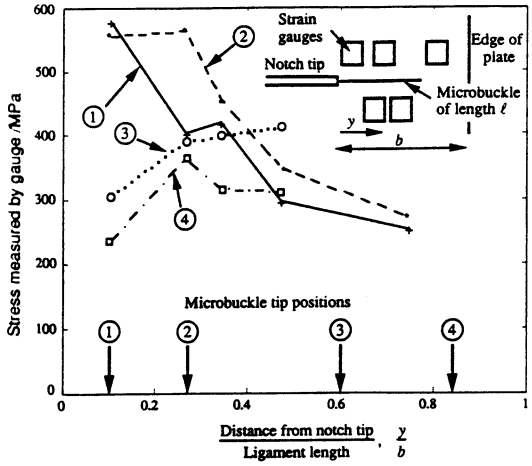

Fig. 12. "Snapshots" of the stress across an unclamped specimen as the microbuckle grows past the strain gauges. The position of gauges on the specimen is shown drawn to scale. Arrows mark the position of the microbuckle tip for each curve. Each curve relates to a particular location of microbuckle tip and shows the axial stress measured by the 5 strain gauges.

At low loads the strain gauge readings varied linearly with load and agreed well with the elastic strain field calculated using finite elements, assuming a sharp notch and no microbuckle damage. On increasing the load further a microbuckle initiated and grew past the strain gauges. The response was now no longer given by the elastic strain field around an undamaged notch. Figure 12 shows "snapshots" of the stress at the strain gauges as the microbuckle grew past them. The successive positions of the microbuckle tip are indicated by arrows. Because the strain gauges were 0.5 mm square, they were not able to resolve the details of the strain field close to the microbuckle tip. However, if the tip of the microbuckle and the tip of the notch are far enough away from the strain gauges and if the strain field is only changing slowly along the microbuckle they give a useful measure of the stress across the microbuckle†. Figure 14 shows that the stress gradient away from notch and microbuckle tips is small. There is substantial variability in readings as the microbuckle

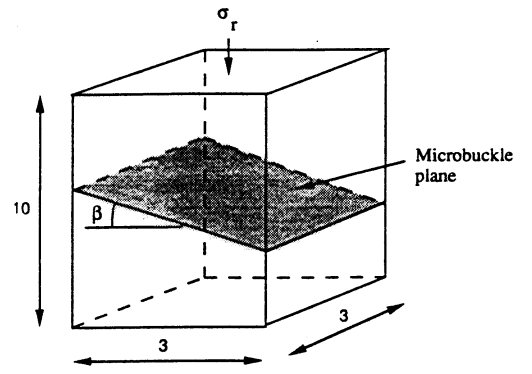

Fig. 13. Micro-compression test specimen. All dimensions are in millimetres.

†Because of the strong anisotropy of the specimen, stresses can diffuse at half the rate parallel to the notch direction as compared with the fibre direction [11]. Hence the strain gauge near the notch tip will not be as affected by the notch tip as it might first appear.

Fig. 14. Multiple kink band formation in an out-of-plane microbuckle. Loading and fibres run in the vertical direction.

traverses the specimens but, when the microbuckle is well past the gauges, the stress across the microbuckle levels out at about 300 MPa. This in-plane stress corresponds to a shear frictional traction on the microbuckle face inclined at 30° to the through-thickness direction of 130 MPa, via a straightforward Mohr's circle construction.

4.2.2. Measurement of the rubble strength of a microbuckled layer. A further estimate of the stress that the microbuckle can carry was obtained by measuring the axial stress that a microbuckled layer could withstand. Two small specimens containing microbuckles across their full sections were cut from an unclamped notched specimen, which had already suffered out-of-plane microbuckling. Although the specimens were completely bisected by an out-of-plane microbuckle, they still retained enough strength to stay intact when handled delicately. The specimens are illustrated in Fig. 12, which also includes approximate dimensions. The specimens were loaded axially in a screw driven test machine: they failed by shear along the microbuckle plane at compressive stresses of 138 and 146 MPa. Since the microbuckles made angles of 23° and 28° to the transverse direction respectively, this corresponds to shear stresses on the microbuckles of 50 and 60 MPa.

The difference between the shear strength estimate of 55 MPa obtained from the micro-compression test and the estimate of 130 MPa from the strain gauge measurements is not clear. However, the fracture surface of the microbuckle in the compression test was smoother than that of the out-of-plane microbuckle in the notched test (as described in Fig. 12). It is conjectured that the shear strength increases with surface roughness. The best estimate of shear and normal strengths is probably somewhere between the two measurements, say 90 MPa. Note that the shear strength of the composite is 90 MPa at a shear strain of about 6%, suggesting that the shear behaviour of the composite determines the bridging stress.

We have assumed that there is continued sliding behind a propagating microbuckle. This has been supported by measurements of the relative displacements across the microbuckle shown in Figs 8 and 9, and discussed in Section 3. To investigate the mechanism of sliding further, another small specimen was cut from an unclamped notched specimen. This specimen was similar to those used for the micro-compression tests, as illustrated in Fig. 12. The small specimen was reloaded compressively *in situ* in the scanning electron microscope, with loading along the original loading direction and parallel to the fibre direction. Sliding across the microbuckle zone was by a combination of two mechanisms:

(i) gross rigid-body sliding of material above the microbuckle band over material below the microbuckle band (with the microbuckle band acting as a rubble zone): and
(ii) multiple kink band formation, with the direction of propagation of the microbuckling normal to that of the initial microbuckle band. This is illustrated in Fig. 14.

Similar views to that shown in Fig. 14 enable us to estimate that the smallest radius of curvature that fibres can withstand before fracture is about 200 μm. If we subtract the small compressive strain on the material of 0.1%, this corresponding to a peak tensile strain in a 5 μm diameter fibre of 1.2%. This is in good agreement with the tensile failure strain for unidirectional material of 1.3–1.5%.

5. APPLICATION TO LAMINATES

While microbuckling is the dominant mechanism of failure in multi-directional laminates, a number of other failure mechanisms operate simultaneously. Previously it has been suggested [9, 13] that the

toughening associated with off-axis splitting, matrix plasticity or delamination could explain the poor agreement between theoretical estimates of the microbuckle toughness based on an infinite-band kink model and measurements of laminate toughness. The results and insight gained from the uni-directional tests can be used to model, in a simple way, the toughness expected from laminates. The comparison is made here for a $[(\pm 45°/0°_2)_3]_s$ laminate containing 50% 0° plies. We assume that the micro-mechanical model found for the out-of-plane microbuckle in the uni-directional material also applies to this laminate. The damage region is modelled using a mode I analysis, with the tip toughness G_t of 11 kJ/m^2 and a bridging stress σ_b across the damage region of 220 MPa. No allowance is made for any difference in toughness between the 0° and the 45° plies. Since microbuckles are observed in the 45° plies this assumption, although no doubt an over-simplification, will serve as a reasonable first approximation.

In the experiments described in this paper microbuckles in uni-directional material propagated stably across the specimen while multi-directional specimens fail catastrophically when the damage zone reaches a critical length. X-ray photographs of specimens with slits just before failure (unreported work from tests described in [8]) show that this critical length is about 2.5 mm for the lay-up under consideration. To estimate the laminate toughness, we find the toughness at the slit in an infinite plate when a critical damage length l_c of 2.5 mm is reached. The large scale bridging model illustrated in Fig. 2(b) will be used. The laminate toughness G_l is made up of contributions from a tip toughness and from bridging tractions [14]

$$G_l = G_t + \sigma_b v \tag{1}$$

where v is the closing displacement at the notch tip with a damage zone of length l_c. v is given by the sum of the displacements due to tractions on the bridging zone of length l_c and due to the tip stress intensity field. These displacements are given by Tada *et al.* [15]†

$$v = \frac{8 l_c \sigma_b}{\pi E'} + \sqrt{\frac{32 G_t l_c}{\pi E'}}. \tag{2}$$

For the laminate considered E' is 73 GPa. Substituting equation (2) into equation (1), we derive an expression for the laminate toughness in terms of the tip toughness, bridging stress, laminate stiffness and critical damage length. This value of the laminate toughness G_l is 29 kJ/m^2, which agrees reasonably with the value of 37 kJ/m^2 found experimentally by Sutcliffe and Fleck [13]. This agreement suggests that toughness due to microbuckling is the dominant toughening mechanism in the laminate.

†For this infinite geometry, isotropic calculations exactly apply to an orthotropic material.

6. CONCLUDING DISCUSSION

Failure in composites can be divided into two phases, an initiation phase and a propagation phase. The work described in this paper has been concerned with propagation. Stable microbuckle propagation in uni-directional carbon fibre-epoxy specimens with a slit has been described. Microbuckling of fibres was either in the plane of the specimen, or out-of-plane, depending on the lateral constraints imposed by small clamping plates on the free surfaces.

Large scale bridging models of in-plane and out-of-plane microbuckles have been described. The in-plane microbuckle is treated as a mode II crack. Sliding behind the crack tip is resisted by a shear stress, estimated from experiments as about 90 MPa. A microbuckle tip toughness of between 10 and 17 kJ/m^2 is inferred from the experiments. The out-of-plane microbuckle is treated as a compressive mode I crack. Out-of-plane displacements at the microbuckle tip allow this apparent over-lap of material. Using a bridging stress of 220 MPa, corresponding to a shear stress of 90 MPa on the slip plane, the tip toughness is inferred from experiments to be about 11 kJ/m^2. Microbuckle closing displacements calculated using the mode I crack model are found to agree well with measurements. This agreement, and the agreement between the inferred tip toughness for in-plane and out-of-plane microbuckles, suggest that it is not necessary to model more accurately the mode III-type conditions at the tip of an out-of-plane microbuckle. This is analogous to failure in sheet metal, where through thickness shear ahead of a crack leads to a mode I fracture.

The details of the microbuckle tip have been investigated by sectioning and by *in situ* tests in a scanning electron microscope. Figures 10 and 11 illustrating the microbuckle tip for the clamped and unclamped specimens respectively, show that the failure mechanisms are similar in both cases. Both develop kink bands with a width of between 25 and 70 μm (5–14 fibre diameters) and with a propagation angle β of between 25 and 30°. A process zone where the fibres switch from being straight to being broken extends about 250 μm ahead of the kink band tip. Unloading considerably straightens these fibres, although some residual waviness is observed for the out-of-plane specimen. Behind the microbuckle tip there is further relative displacement across the kink band both due to sliding in the fracture plane and due to the formation of multiple kink bands.

The large scale bridging model found for uni-directional material is applied, in a simple way, to laminate failure. The tip toughness and bridging stress found in the out-of-plane microbuckle are applied to a $[(\pm 45°/0°_2)_3]_s$ laminate. The predicted laminate toughness is about 29 kJ/m^2, which agrees reasonably with the measured value of 37 kJ/m^2.